# Ionizing Radiation induces cells with past caspase activity that contribute to the adult organ in *Drosophila* and show reduced Loss of Heterozygosity

Sarah Colon Plaza and Tin Tin Su

Department of Molecular, Cellular and Developmental Biology, University of Colorado at Boulder, CO, 80309-0347

**Abstract**

There is increasing recognition that cells may activate apoptotic caspases but not die, instead displaying various physiologically relevant consequences. We know very little, however, of mechanisms that underlie the life/death decision in a cell that has activated apoptotic caspases. By optimizing a published reporter of past caspase activity, we have been able to visualize such cells that results specifically from exposure to ionizing radiation in *Drosophila* larval wing discs. We found that cells with X-ray-induced past active caspases (XPAC) do not arise at random but are born at specific locations within the developing wing imaginal discs of *Drosophila* larvae. Reduction of apoptotic signaling reduced the prevalence of XPAC cells. Yet, XPAC cells appear in stereotypical patterns that do not follow the pattern of IR-induced apoptosis, suggesting additional controls at play. Functional testing identified the contribution by Wg (Wnt1), Notch and Ras signaling in this process. By following irradiated larvae into adulthood, we found that XPAC cells contribute to the adult wing. To address the relationship between XPAC and genome stability, we combined a reporter for past caspase activity with *mwh*, an adult marker for Loss of Heterozygosity (LOH). Our data suggest that non-lethal caspase activity safeguards the genome by facilitating DNA repair and reducing LOH after transient exposure to X-rays, identifying a physiological role for non-lethal caspase activity during recovery from radiation damage.

**Author Summary**

Cells may activate enzymes needed for apoptosis, a form of cell death, yet not die. We found that cells that lived through the activation of apoptotic enzymes after exposure to ionizing radiation show reduced aberrations in their genomes, suggesting that a near-death experience may benefit the cell.

**Fit for PLoS Genetics**

We make use of *Drosophila* genetics to address the survival and the fate of cells with past caspase activity, a phenomenon of broad interest. Therefore, this work is a good fit for the readership of PLoS Genetics.

33 **Introduction**

34 Caspases are a family of cysteine proteases that are conserved in metazoan. Some members of the
35 caspase family function in non-apoptotic processes such as cytokine maturation and innate immunity
36 whereas other members such as Caspases 3 and 7 degrade proteins to execute apoptosis, to be called
37 'apoptotic caspases' here (for reviews, [1, 2]). An exciting emerging field is based on the recognition that
38 cells may activate apoptotic caspases but not die, instead displaying various physiologically relevant
39 consequences (for reviews, [3-6]). For example, apoptotic caspases serve non-apoptotic purposes during
40 organism development that include axon pruning, stem cell differentiation, reduction of the cytoplasm
41 during sperm maturation, and elimination of the nuclei during the maturation of vertebrate lens cells
42 and Red Blood Cells. Cells survive caspase activation that occurs naturally during each of these
43 processes. Past caspase activation is also associated with cells that undergo anastasis, a process in which
44 a cell returns to life from the brink of apoptotic death [4, 7-9]. Anastasis is observed in cultured cells
45 exposed to a variety of death stimuli including ethanol [10], a broad-spectrum kinase inhibitor
46 Staurosporine and a small molecule BCL-2 antagonist [11], or ion beam radiation [12]. Removal of death-
47 inducing stimuli before apoptosis is completed allows some cells to recover even after displaying such
48 apoptotic features as cleaved active caspases, Mitochondrial Outer Membrane Permeabilization
49 (MOMP), or flipping of phosphatidylserine onto the outer cell membrane. Cells that underwent
50 anastasis are not only alive but are capable of proliferation and initiating tumors. Both anastasis and
51 developmental caspase activation produce cells with past caspase activity. But the latter are not
52 necessarily products of anastasis because many such cells may not have initiated apoptosis.

53

54 To study the non-apoptotic role of apoptotic caspases, we need to be able to detect cells that activated
55 caspases but did not die. Two genetic reporters for past caspase activation in living cells have been
56 described in *Drosophila melanogaster* and both rely on caspase-mediated permanent changes in the

genome that result in constitutive GFP expression [13, 14]. At the core of CasExpress and Caspase Tracker biosensors is transcriptional activator GAL4 that has been modified with a cell-membrane tether. The tether includes a recognition sequence, DQVD, for effector caspase Drice (*Drosophila* caspase 3/7). Upon caspase activation, the tether is cleaved to allow GAL4 to enter the nucleus and activate transcription. Use of this in conjunction with the G-trace lineage tracing system [15] allows for real-time detection via UAS-RFP and lineage marking via UAS-FLP recombinase; FLP catalyzes a recombination event to cause ubiquitous and permanent GFP expression. Both CasExpress and Caspase Tracker show that non-lethal apoptotic caspase activity is widespread in nearly every tissue during *Drosophila* development [13, 14]. The specificity of biosensors is demonstrated by control sensors with a DQVD->DQVA mutation that abolished reporter activity. These findings agree with the body of evidence for non-lethal activation of apoptotic caspases in multiple tissues in various metazoan model organisms.

We wanted study cells with past caspase activity induced not by developmental events but by ionizing radiation (IR). IR is one of three main modalities in cancer therapy, the others being surgery and chemotherapy. The success of radiation therapy of cancer relies on IR's ability to induce apoptosis. Therapy failure can result if cells initiate but do not complete apoptosis after IR exposure, making it important to understand molecular mechanisms that regulate the production of such cells. We have found it challenging to use CasExpress and Caspase Tracker to detect IR-induced non-lethal caspase activation because of constitutive signal from these biosensors. Even when a temperature-sensitive repressor of GAL4, GAL80$^{ts}$, was used to limit GAL4 activity temporally, we still observed GFP+ cells in mock-irradiated larval wing discs [16]. Here, we report an optimized temperature shift protocol that out-performs our published protocol by increasing the ratio of IR-induced to constitutive signal from ~2-4 to ~20. The optimized protocol allows us to detect cells with past caspase activity that results specifically from exposure to X-rays. We found that cells with X-ray-induced past active caspases (XPAC) do not arise

81 at random but are born at specific locations within the developing wing imaginal discs of *Drosophila*
82 larvae. Reduction of apoptotic signaling reduced the prevalence of XPAC cells. Yet, XPAC cells appear in
83 stereotypical patterns that do not follow the pattern of IR-induced apoptosis, suggesting additional
84 controls at play. The prevalence and stereotypical pattern of XPAC cells change with development such
85 that less developed wing discs show greater XPAC prevalence compared to more developed wing discs.
86 Functional testing identified the contribution by Wg (Wnt1), Notch and Ras signaling in XPAC cell
87 number. By following irradiated larvae into adulthood, we show that XPAC cells contribute to the adult
88 wing. Anastasis has been associated with increased genome instability in immortalized mammalian cells
89 [9, 11, 12]. On the other hand, wide-spread non-lethal caspase activity is detected during normal
90 *Drosophila* development, raising the possibility that such activity may be neutral or even beneficial to
91 normal cells. Using our protocol in conjunction with a cell-autonomous marker for Loss of
92 Heterozygosity (LOH), *mwh*, we were able to address this question. Our data suggest that non-lethal
93 caspase activity safeguards the genome by facilitating DNA repair and reducing LOH after transient
94 exposure to X-rays.
95
96 **Results**
97 *Optimizing temperature shift conditions to detect cells with past IR-induced caspase activity*
98 In our published studies to detect X-rays-induced past caspase activity (XPAC) using Caspase Tracker, we
99 raised the larvae at 18°C and shifted them to 29°C to inactivate GAL80$^{ts}$ from 0 to 6h after irradiation
100 with 4000R (40Gy) of X-rays [16] (Fig. 1A, T=29°C). 4000R is typically used in *Drosophila* because almost
101 all wild type larvae eclose into adult flies at this dose but about half of them die soon after, making it the
102 $LD_{50}$ dose. We reason that this dose causes sufficient damage but is still compatible with mechanisms
103 that allow survival. We chose 0-6h after IR because it includes the peak of caspase activation. After
104 exposure to 4000R of X-rays, pro-apoptotic genes *hid* and *rpr* that are needed for IR-induced caspase

105 activation are transcriptionally induced at 2h after IR [17]. Caspase cleavage is detectable at about 3h
106 after IR as is apoptosis as detected by staining with the vital dye Acridine Orange; AO stains apoptotic
107 and not necrotic cells in *Drosophila* [18]. By 4h after IR, *hid/rpr* expression has declined compared to the
108 2h time point, although cleaved caspases and AO staining remain visible for up to 24h after [17]. Based
109 on these results, we are using a 6h window immediately after IR to capture the bulk of IR-induced
110 caspase activation.
111
112 Our published experiments with Caspase Tracker [20] are reproduced here (Fig. 1B, the first two
113 datasets) and expanded to include CasExpress (Fig. 1C-D'; quantified in Fig. 1B, middle two datasets).
114 Even with limited (6h) activation of GAL4 at 29°C, wing discs from unirradiated larvae show GFP+ cells
115 (Fig. 1C', quantified in Fig. 1B, the first two -IR datasets). The GFP+ area increased significantly with
116 irradiation (Fig. 1D', quantified in B), for both Caspase Tracker and CasExpress. IR increased the mean
117 disc area with Caspase Tracker>GFP by about 3-fold and CasExpress>GFP by about 4-fold. This means
118 about 66% of Caspase Tracker>GFP cells and about 75% of CasExpress>GFP cells observed in irradiated
119 discs are X-ray-induced while the remainder are from developmental caspase activation. We wanted to
120 improve the experimental conditions such that nearly all GFP+ cells in irradiated discs are due to IR. To
121 this end, we examined the effect of different incubation temperatures after IR in the protocol in Fig. 1A
122 (Figure 1 E-G'). We used CasExpress in these efforts because its datasets show smaller variance than
123 Caspase Tracker (Fig. 1B). As we increased the incubation temperature from 18°C, we found that we
124 could go as high as 26°C and still keep the CasExpress>GFP area to near zero in unirradiated discs (Fig.
125 1G', quantified in B). At T=26°C, irradiation increased the GFP+ area significantly (Fig. 1H', quantified in
126 B). A control CasExpress sensor with a DQVD->DQVA mutation showed no GFP+ cells even with
127 irradiation (compare Fig. 1I to H'), indicating that GFP+ cells report effector caspase activity specifically.
128 Returning the larvae back to 18°C immediately after irradiation, that is, without any temperature shift,

129 eliminated GFP+ cells (Fig. 1J), indicating that production of GFP+ cells is GAL4-dependent. Because of
130 low GFP+ area in -IR discs at 26°C, the 'signal to noise' ratio was greatest under these conditions: a 20-
131 fold increase in mean GFP+ area between 0R and 4000R. Therefore, we could be confident that most
132 (>90%) of GFP+ cells we see in +IR discs were cells with X-ray-induced past active caspases (XPAC).
133 Subsequent experiments use the protocol in Fig. 1A with T=26°C.
134
135 XPAC *cells proliferate*
136 The data in Fig. 1 were from 3 days after irradiation. To study GFP+ XPAC cells soon after they form, we
137 performed a time course (Fig. 2). GFP+ cells were not observed at 6h after IR but were readily detectable
138 at 24h after IR (Fig. 2A). At this time, most GFP+ cells were either singlets (arrow) or in small groups of 2-
139 5 cells (arrowhead). At 48h after irradiation, single GPF+ cells were rare and most cells were in clones of
140 4-30 cells each (Fig. 2B). Clone size increased further at 72h after IR, the last time point taken before we
141 lost the larvae to pupariation (Fig. 2C). We conclude that XPAC cells are capable of clonogenic
142 proliferation. Real time marker RFP was not observed (Fig 2. A'', B'', C''), presumably because the return
143 to 18°C restored GAL80$^{ts}$ and repressed GAL4.
144
145 ***The prevalence and the location of XPAC cells change with development***
146 We next addressed the factors that influence the production of XPAC cells. Our collection of larvae
147 spanned 24h in age. As such, we observed a range of developmental stages, that is, discs of different
148 sizes and degree of epithelial folding (Figure 3A-D; arrowheads point to increasing folding in more
149 developed discs). We noticed three trends in the prevalence and the location of GFP+ cells at 24h after
150 IR. First, smaller discs showed more GFP+ area relative to the disc size than larger, more developed discs
151 (compare Fig. 3D' to A'). A plot of % disc area that is GFP+ against disc size illustrates this trend (Fig. 3F
152 '6-7d at IR'). The area serves as surrogate for cell number and is justified for a single layer epithelium.

153 4000R of X-rays stop the cell cycle via checkpoint activation, with S phase and mitosis resuming at about
154 6h after irradiation [19]. Cell doubling times in 3rd instar wing discs average 12h [20]. Therefore, at 24h
155 after irradiation when we quantify XPAC cells, cells would have divided on average just once, which can
156 be seen as the appearance of singlets (arrow) and doublets (arrowhead) in Fig. 2A. Zero to one division
157 is insufficient to form scorable clones, which is why we measure the area rather than clone number.
158
159 We interpret the size-dependence to mean that as the disc increased in developmental age, X-rays were
160 able to induce fewer cells that activated caspases but survived. This correlation was confirmed by aging
161 the larvae for an additional 24h at 18°C before irradiation but treating them as in Fig. 1A otherwise. This
162 produced larger, more developed discs. Importantly, the same relationship between disc size and %
163 GFP+ area was observed in the older cohort (Fig. 3F, '7-8d at IR'), except that overall values shifted to
164 the right as expected for larvae that were one day older. An alternate method of data analysis, which
165 has been used in the literature to separate wing discs according to development [21], led to the same
166 conclusion. When discs with no epithelial folds (younger/less developed discs, as shown in Fig 3A and
167 3B) and discs with epithelial folds (more developed discs, as shown in Fig. 3C and 3D) were analyzed
168 separately, the %GFP+ area was lower for more developed discs (Fig. 3G), further supporting the idea
169 that the prevalence of XPAC cells changes with development.
170
171 The second trend we saw was that the distribution of GFP+ cells in each disc was not homogenous. The
172 notum (future body wall or 'n' in Fig. 3A') had fewer GFP+ cells than the future wing ('w' in Fig. 3A'
173 includes the hinge and the pouch). This was true regardless of disc size.
174

175 The third trend we saw was that when the number of GFP+ cells declined in larger discs, their loss was
176 not evenly distributed throughout the disc. Instead, the distal pouch (* in Fig. 3A', B', C') became clear of
177 GFP+ cells before the rest, leaving a ring of GFP+ cells (Fig. 3C', arrows).
178
179 ***Apoptosis signaling modulates XPAC cell number***
180 To identify mechanisms that influence whether a cell with active caspases lives or dies, we targeted
181 molecules involved in the apoptotic signaling pathway. We addressed the cell-autonomous requirement
182 by expressing each transgene for 6h after IR under UAS control, which means only in cells that have
183 activated caspases and translocated GAL4 into the nucleus as part of the CasExpress system. Thus, we
184 are asking what keeps cells alive after they began to activate apoptotic caspases. We analyzed our data
185 based on the stage of development, separating less developed discs (no epithelial folds) from more
186 developed discs (epithelial folds). We increased apoptotic signaling by expressing pro-apoptotic genes
187 *hid* and *rpr* together or *rpr* alone. We decreased apoptotic signaling by expressing a dominant negative
188 version of apical caspase Dronc in which an essential cysteine in the active site has been mutated to an
189 alanine or viral caspase inhibitor p35 that inhibits effector caspases. We used also heterozygotes for the
190 H99 chromosomal deficiency that removes *hid*, *rpr* and *grim* and has been shown to reduce and delay
191 IR-induced apoptosis [17]; the effect of H99 would be throughout the organism and not just cell-
192 autonomous. Both increased and decreased apoptotic signaling led to reduced XPAC prevalence (Fig
193 3H). The seemingly paradoxical finding can be explained by the threshold model for apoptotic induction
194 wherein cells must accumulate a certain level of effector caspase activity to die [22]. Increasing effector
195 caspase activity with UAS-*hid*/*rpr* would push cells over the threshold, reducing the number of GFP+
196 cells that activated apoptotic caspases but lived. Reduction of apoptotic caspase activation with H99
197 would reduce effector caspase activity, preventing some cells from activating CasExpress, thus also
198 reducing the number of GFP+ cells. The ability of $Dronc^{DN}$ and p35 to reduce XPAC prevalence when

199 expressed under the control of CasEx-GAL4 suggests that not all CasEx-GAL4 that localizes to the nucleus
200 succeeds in facilitating a recombination event to result in permanent GFP expression. Instead, a positive
201 amplification loop wherein an active caspase cleaves to activate more caspases, which can be blocked
202 by Dronc$^{DN}$ or p35, may be needed to generate a GFP+ XPAC cell.
203
204 The effect of altering apoptotic signaling on XPAC cells was more pronounced for less developed discs
205 (Fig 3H vs. I). The effect of *hid*, *rpr* and Dronc$^{DN}$ were still significant in more developed discs but H99 and
206 p35 did not produce significant effects (Fig 3I). We do not know the reason for this but it is possible that
207 while 2 copies of *hid*, *rpr* and *grm* are needed to activate CasEx to the level that results in permanent
208 GFP expression in younger discs (hence the sensitivity to H99), only one copy is sufficient in more
209 developed discs.
210
211 ***Developmental changes in XPAC induction does not correlate with apoptosis or cell proliferation***
212 We next addressed why the prevalence of GFP+ cells decline in more developed discs. One possible
213 explanation is that cells in more developed discs are post-mitotic; non-dividing cells are known to be
214 refractory to apoptosis, for example in the eye disc [23]. Staining with an antibody to phospho-Histone
215 H3, a mitotic marker, ruled out this possibility (Fig 4A-C''). At 24h after IR when cells have already
216 recovered from checkpoint arrest [19], all discs show robust and wide-spread mitoses regardless of
217 whether they also display robust XPAC prevalence (Fig 4A''-B'') or few detectable GFP+ cells (Fig 4C'').
218 We note robust mitotic activity in the notum (arrows) and the pouch (between dashed lines in Fig 4C-
219 C'') that includes the future Zone of Non-Proliferating Cells (ZNC). The ZNC is comprised of only two
220 rows of cells that flank the dorsal/ventral boundary (D/V) and the arrest occurs in late 3$^{rd}$ instar stage
221 whereas clearing of XPAC cells is observed in a larger area of the pouch or throughout the disc. Disc
222 regional difference in XPAC prevalence, notum versus wing in Fig 3B' for example, also does not

223 correlate with regional difference in cell doubling times reported in the literature [21]. We conclude that
224 proliferation state cannot explain the reduction of XPAC cells in more developed discs.
225
226 Another possible reason for the decline in XPAC prevalence in more developed discs is that X-rays were
227 less efficient at inducing caspase activity. A published study found that IR-induced apoptosis becomes
228 restricted in the wing discs of wandering stage larvae, for example, with cells along the D/V boundary
229 becoming refractory to apoptosis [24]. On the other hand, we have not observed such restrictions in
230 feeding stage larvae that we use in our experiments with the exception of the hinge. We have shown
231 before that cells of the hinge in feeding stage larvae are protected from IR-induced apoptosis by the
232 combined action of Wg and STAT while the rest of the wing disc cells are sensitive to IR-induced
233 apoptosis [23]. Staining for a cleaved active effector caspase or with a vital dye confirm this finding (Fig 4
234 D-J). Cleaved Dcp1 signal is absent without irradiation (S1 Figure A-A'') but is readily discernable in
235 irradiated discs regardless of whether they show robust XPAC induction (Fig 4D'' and E'') or only a few
236 detectable GFP+ cells (Fig 4F''). Disc areas with Dcp1 signal includes the notum (arrow) and the distal
237 pouch (*) that display reduced XPAC prevalence as the discs mature. That IR induces wide-spread cell
238 death at developmental stages we study was confirmed by staining wing discs at with 4 h after IR with a
239 vital dye Acridine Orange (AO), which in Drosophila reports apoptosis [18] (Fig 4G-H; the brackets
240 indicate the hinge cells that we showed before are refractory to IR-induced apoptosis [23]). We
241 conclude that while apoptotic caspase activity is necessary to generate XPAC cells (Fig 3), it is not
242 sufficient to explain the spatiotemporal distribution of XPAC cells, which does not match the
243 spatiotemporal distribution of IR-induced caspase activation. We infer that other mechanisms operate
244 on top of caspase activation to decide whether a cell with active caspases live or die.
245
246 ***Developmental Signaling pathways modulate XPAC prevalence***

247 The changing pattern of XPAC cells as discs mature suggests that developmental signaling pathways may
248 contribute to the survival of XPAC cells. We tested the role of Wg and N because XPAC cells appear to
249 'clear' from the distal pouch (* in Fig 3, 4, 5) where N drives Wg expression (yellow arrowhead in Fig 5C)
250 suggesting that these activities reduce XPAC number. On the other hand, XPAC cells persist near the Wg
251 Inner Ring (white arrowhead in Fig 5C), suggesting that Wg promotes XPAC survival. To test these ideas,
252 we expressed UAS-Wg or its inhibitor UAS-Axin for 6h after irradiation in CasExpress-GAL4-active cells as
253 we did for apoptotic pathway components in Fig 3. We find that either increasing or inhibiting Wg
254 signaling transiently had the same effect of lowering XPAC prevalence in less developed discs (a
255 representative disc with no folds is shown in Fig 5E, quantified in F). Likewise, transient manipulations of
256 N signaling with a constitutively active N (UAS-$N^{ICD}$) or a dominant negative inhibitor (UAS-$mam^{\Delta}$) also
257 had the same effect of lowering XPAC prevalence (Fig 5E). These results are reminiscent of how
258 increasing apoptotic functions (with *hid* and *rpr*) and decreasing apoptotic functions (with $Dronc^{DN}$ or
259 p35) both lowered XPAC prevalence in less developed discs (Fig 3H). Given the known anti-apoptotic
260 role of Wg [23] and the ability of N to activate Wg, a threshold model for apoptosis that could explain
261 the results with *hid*/*rpr* and Dronc could also be used to explain the Wg/N results. Specifically, reducing
262 Wg signaling may drive cells over the threshold while increasing Wg signaling may prevent caspase
263 activation, both of which could reduce XPAC number. We tested also the effect of Ras signaling because
264 it is known to restrict IR-induced apoptosis to intervein regions in the pouch in wandering stage larvae
265 [24]. Expression of a constitutively active $Ras^{G12V}$ mutant lowered XPAC prevalence in less developed
266 wing discs (Fig 5F). Ras/MAPK is known to inhibit caspase activation, by direct phosphorylation and
267 inhibition of Hid during Drosophila eye development for example [25], which could explain how it can
268 decrease XPAC prevalence.
269

270 As in the case of H99 heterozygotes, manipulation of Wg, N and Ras had less effect on XPAC cells in
271 more developed discs (Fig 5G). The only statistically significant effect, although small, was seen with
272 UAS-Wg, which increased XPAC prevalence. This is opposite of the case in less developed discs where
273 UAS-Wg lowered XPAC prevalence. We do not know why Wg overexpression results in opposite effects
274 on XPAC cells depending on the developmental stage but note that context-dependent pro- and anti-
275 apoptotic roles have been shown for another conserved factor, E2F1, in Drosophila wing discs [24].
276
277 ***Cells with past caspase activity show reduced IR-induced LOH***
278 We next asked what the consequences of past IR-induced caspase activity is on cells. This question has
279 been addressed in cultured human cells using $^{56}$Fe ion particle radiation, a type of IR. Cells exposed to
280 0.5 Gy (500R) of particle radiation show persistent caspase activation for up to two weeks without dying
281 [12]. Under these conditions, caspase activity promoted DNA breaks and induced oncogenic
282 transformation. X-rays on the other hand induce transient caspase activation, with DNA breaks clearing
283 within 24h in larval wing discs [19, 23]. To ask what the consequences of transient non-lethal caspase
284 activation is in this context, we assayed for Loss of Heterozygosity using *multiple wing hair* as a marker.
285 *mwh* resides at the tip of chromosome III. Homozygosity of recessive alleles increases the number of
286 hairs per wing cell due to defective actin organization [26]. Heterozygotes appear wild type and allows
287 the detection of loss of the wild type allele through LOH. We have shown previously that *mwh* LOH is
288 absent without irradiation but is induced when larvae are irradiated with 4000R of X-rays [27].
289
290 We were able to use *mwh*, which produces an adult phenotype, because GFP+ XPAC cells survive into
291 adulthood and appear in adult wings an IR-dependent manner (Fig. 6). This was true regardless of larval
292 age (6-7d or 7-8d) at the time of irradiation (see Fig. 3F for corresponding 6-7d and 7-8d XPAC data in
293 larval discs). At higher magnification, it is possible to assign GFP+ cells to each surface of the wing (arrow

294 versus arrowhead in Fig. 6G) and assign the *mwh* and GFP status to individual cells (Fig. 6H, 3 GFP+ cells
295 are shown inside dashed lines). Quantification of the GFP- or GFP+ area of the wing that is also *mwh*
296 shows that GFP+ areas show fewer *mwh* cells compared to GFP- areas of the same wing (Fig. 5I). This
297 was true regardless of larval age at the time of irradiation. We conclude that cells with XPAC show
298 reduced LOH compared to those without. To address a possible explanation for this finding, we
299 monitored DNA double strand breaks (DSB) induced by X-rays under the same experimental conditions.
300 We and others have shown before that 4000R of X-rays induce DSBs throughout all cells of the wing disc
301 that can be detected with an antibody to phosphorylated histone variant H2Av (x in mammals) (γ-H2Av;
302 reproduced in S1 Figure B-C' at 4h after irradiation). A published time course demonstrate that γ-H2Av
303 signal is reduced to near-background levels 24h after irradiation suggesting that cells have completed
304 repair by this time [19, 23]. Consistent with these data, at 20-22h after IR, only a subset of cells show γ-
305 H2Av staining (Fig 6 J-L''''), which we interpret as cells that have yet to complete DNA repair.
306 Appropriate for our purposes, CasExpress>GFP signal becomes detectable at this time. Co-imaging in the
307 same discs show mutual exclusion of GFP and γ-H2Ax signals with rare cells that show both signals
308 (arrowheads in Fig 6J''''). We interpret these results to mean that XPAC cells complete DNA repair more
309 efficiently than their GFP-counterparts. Possible mechanisms are discussed below. More efficient repair
310 in XPAC cells, we propose, could explain the observed reduction in LOH.
311
312 **Discussion**
313 We report here a study of cells with X-ray induced past active caspases (XPAC) during wing development
314 in *Drosophila*. An optimized temperature shift protocol allowed us to minimize cells with spontaneous,
315 developmental caspase activity and to focus specifically on XPAC cells. Such cells, we found, were able to
316 proliferate and contribute to the adult organ.
317

318 We are aware of three published studies that addressed the relationship between past caspase activity
319 and genome stability. In a study by Tang and colleagues, primary mouse liver cells and 3T3 immortalized
320 mouse embryonic fibroblast cell line were treated for 5h with 4.5% ethanol, an apoptosis inducer [9].
321 Three days after the treatment, cells showed increased abnormal chromosome number and appearance
322 (for both cell types) and increased colony formation that is indicative of oncogenic transformation (for
323 3T3 cells). In another study, Ichim and colleagues treated HeLa, U2OS, and other cancer cell lines for 3h
324 with a BH3 mimic ABT-737, to induce limited Mitochondrial Outer Membrane Permeabilization or
325 'minority MOMP' [11]. MOMP is an early step in apoptosis induction but with limited MOMP in these
326 experiments, cells did not die but displayed DNA fragmentation as detected by staining for γ-H2AX and
327 by comet assay. Incubation with a pan-caspase inhibitor prevented DNA fragmentation in these
328 experiments, implicating caspase activity as the cause for DNA fragmentation. ABT-737 also promoted
329 colony formation induced by KRAS/E1A in mouse embryo fibroblasts (MEF) and tumor formation by
330 MEFs that are null for tumor suppressor p19ARF.
331
332 Finally, in the only published study to use IR to induce sub-lethal caspase activity and assay the effect on
333 genome stability, Liu and colleagues exposed MEFS and immortalized human epithelial cells and
334 fibroblasts (MCF10A and IMR90) to $^{56}$Fe ion particle radiation [12]. Cells exposed to 0.5 Gy (500R) of $^{56}$Fe
335 radiation showed persistent caspase activation as assayed by a live caspase activity reporter, for up to
336 two weeks without dying. These cells also displayed γ -H2AX and DNA fragmentation as assayed by
337 comet assays, also for two weeks after irradiation. $^{56}$Fe-irradiated MCF10A cells with high caspase
338 reporter activity formed colonies in soft agar compared to irradiated cells with low reporter activity.
339 Inhibition of caspase 3 using shRNA or a dominant negative construct reduced the colony number,
340 suggesting that caspase activity was causing transformation.
341

342 We found that past caspase activity resulted in reduced IR-induced LOH in *Drosophila* wings. Classical
343 studies in Drosophila demonstrate that mitotic recombination makes only a minor contribution to IR-
344 induced LOH; most LOH cells were in single clones rather than twin spot products expected for mitotic
345 recombination [28]. Although the exact molecular mechanism remains to be determined, LOH serves as
346 a useful quantitative readout of IR-induced genetic abnormalities. While contrary to the above-
347 described results in mammalian cells, our LOH result is consistent with the published reports that non-
348 lethal caspase activity is wide-spread in *Drosophila*. Both CasExpress and Caspase Tracker are active in
349 nearly every tissue during *Drosophila* development [13, 14]. This agrees with the body of evidence for
350 non-apoptotic roles of apoptotic caspases in multiple tissues in various metazoan model organisms.
351 Clearly, caspases activity in these situations is not causing DNA fragmentation or else it would have been
352 detected in multiple studies that monitored DNA breaks (e.g., [19, 23]). We interpret our data to mean
353 that non-lethal caspase activity protects the genome from X-ray-induced chromosome breaks. One
354 possible reason is that unlike with $^{56}$Fe radiation, X-ray-induced DNA breaks are cleared within 24h in
355 larval wing discs as assayed by γ -H2Av, even with much higher IR doses of 4000R (40 Gy) [19, 23].
356 Therefore, it is possible that DNA repair is more efficient in cells of the wing discs and that in this
357 context, non-lethal caspase activity is beneficial. Co-staining for γ-H2Av shows mutual exclusion with
358 GFP, supporting this idea (Fig 6J-K). The question then is, how might past caspase activity help reduce
359 LOH in the wing discs? Caspase-driven cellular transformation in the above cited studies was proposed
360 to occur because caspases unravel the genome to allow access to oncogenic transcription factors such
361 as KRAS/E1A used in these studies [12]. Endonuclease G was found to act downstream of caspases in
362 cellular transformation by $^{56}$Fe. If a similar situation occurs in the wing disc, caspase activity could make
363 the genome more accessible to DNA repair enzymes instead of transformation factors. In other words,
364 consequences of non-lethal caspase activity may depend on the cellular context, specifically, which
365 proteins are present and active to access the DNA. In cells predisposed to transformation such as

366 immortalized cell lines, the outcome may be transformation. In non-immortalized cells or cells that lack
367 transformation factor but are robustly expressing DNA repair enzymes as part of DNA Damage
368 Responses, then increased repair may be the outcome to reduce IR-induced LOH.
369
370 Our published studies have addressed the role of apoptotic caspases in LOH and found both positive and
371 negative inputs [27]. Briefly, cells with X-ray-induce LOH are detectable by 48h after IR in larval wing
372 discs but are culled over the next 24h. This culling requires apoptosis such that H99/+ discs show more
373 LOH clones at 72h after IR. Individual clones in H99/+ discs, however, are smaller than in wild type,
374 suggesting that apoptosis is required for LOH clones to expand, presumably by apoptosis-induced
375 compensatory proliferation. The net result is reduced total LOH area in H99/+ larval wing discs and adult
376 wings. $Dronc^{DN}$ produced similar results. Reduced LOH [27] and reduced XPAC (this study) in H99/+
377 mutants seems contradictory to the finding that XPAC cells show reduced LOH. We note, however, that
378 the effect of caspases on LOH in published studies is proposed to be via apoptosis (to cull LOH cells or
379 promote compensator proliferation) whereas their role in producing XPAC cells requires that they fail to
380 induce cell death.
381
382 We do not know if XPAC cells we detect with a GFP reporter are products of anastasis. To be able to tell,
383 we need to know how far down the apoptosis pathway XPAC cells had gone, which cannot be discerned
384 with biosensors for past caspase activity. The induction of XPAC cells, we found, was sensitive to
385 developmental stage and showed stereotypical patterns in the developing wing disc. These new findings
386 suggest that local differences in gene expression or differentiation state provide a layer of control, which
387 operates on top of required apoptotic caspase activity, to generate XPAC cells. Specifically, we find that
388 optimal levels of Wg and N are needed as either increasing or decreasing each can lower XPAC
389 prevalence. Furthermore, their importance is greater in less developed discs. Lower XPAC prevalence we

390 see after inhibition of Wg or N is unlikely to be indirect via delayed development; if so, we expect XPAC
391 prevalence to increase because less developed discs show more XPAC.
392
393 A recent paper addressed the genetic basis for the prevalence of cells with past caspase activity using
394 the CasExpress system also used here [29]. The primary focus was on developmental CasExpress signal
395 in the wing discs observed without external insults such as radiation or heat shock, which we have taken
396 care to avoid in order to focus on X-ray-induced CasExpress (Fig 1). The study identified a requirement
397 for apical caspase Dronc in developmental CasExpress signal generation, similar to what we see for
398 XPAC. p35 reduced developmental CasExpress signal, which is also similar to what we see for XPAC. A
399 focused RNAi screen in the published study identified Akt and transcription factor dCIZ1 as new
400 regulators of developmental CasExpress induction. Further testing demonstrated a role for dCIZ1 also in
401 surviving executioner caspase activation by heat shock, oncogenic stress and X-rays. More striking, the
402 published study identified a role for oncogenic Ras in preserving cells that expressed developmental
403 CasExpress; expression of $Ras^{V12}$ in the posterior compartment of wing discs increased CasExpress>GFP
404 area by about 2-fold. This is the opposite of what we see; $Ras^{V12}$ reduced XPAC prevalence in less
405 developed discs and had no effect in more developed discs (Fig 5). We conclude that developmental
406 CasExpress induction and XPAC show similar as well as different requirements and represent two
407 distinct cellular responses to executioner caspase activity.
408
409 **MATERIALS AND METHODS**
410 ***Drosophila* stocks**
411 *Drosophila* stocks used in this work are published, available from public stock centers, or both. All stocks
412 used are listed in S1 Table. These include (BL=Bloomington Stock number): G-trace (BL28280),
413 CasExpress (BL65419), CasExpress DQVA control (BL65420), Caspase Tracker [14], $mwh^1$ (BL549), tubP-

414 GAL80$^{ts}$ on Chromosome III (BL7017) , UAS-p35 (BL5073), UAS-hid/rpr and UAS-rpr (BL5823) [30], UAS-
415 Wg [31], UAS-Axin (BL7225), UAS-Dronc$^{DN}$ [32], UAS-Ras$^{V12}$ (BL64195), UAS-Notch$^{ICD}$ (BL26674), UAS-mam$^{\Delta}$
416 (BL26672) and chromosome deficiency H99 (BL1576). To use in the experiments, the following stocks
417 were generated using standard *Drosophila* techniques:
418 Caspase Tracker/CyO-GFP; GAL80$^{ts}$/GAL80$^{ts}$
419 Caspase Tracker/CyO-GFP; mwh$^{1}$/TM6 Tb
420 G-trace/CyO-GFP; UAS-X/TM6 Tb where X was UAS-Wg, UAS-Axin, UAS-p35, UAS-Dronc$^{DN}$, UAS-
421 Ras$^{V12}$, UAS-Notch$^{ICD}$, UAS-mam$^{\Delta}$, or H99
422 G-trace/CyO-GFP; GAL80$^{ts}$/GAL80$^{ts}$
423 UAS-hid, UAS-rpr/UAS-hid, UAS-rpr or Y; G-trace/CyO-GFP
424 UAS-rpr/UAS-rpr or Y; G-trace/CyO-GFP
425 The stocks were maintained on Nutri-Fly Bloomington Formula food (Genesee Scientific) at 25°C. After
426 crossing virgins and males, the adults were fed on Nutri-Fly German Formula food (Genesee Scientific)
427 for 3 days at 25°C to boost egg production, before transferring them to 18° for embryo collection.
428
429 **Larvae culture, temperature shift and irradiation**
430 Embryos were collected and larvae were raised on Nutri-Fly Bloomington Formula food (Genesee
431 Scientific) at 18°C. The cultures were monitored daily for signs of crowding, typically seen as 'dimples' in
432 the food surface as larvae try to increase the surface area for access to air. Cultures were split at the first
433 sign of crowding.
434 Larvae in food were placed in petri dishes and irradiated at room temperature in a Faxitron
435 Cabinet X-ray System Model RX-650 (Lincolnshire, IL) at 115 kV and 5.33 rad/sec. Immediately after
436 irradiation, larvae in food were returned to new vials and placed in a constant temperature bath filled
437 with Lab Armor beads (ThermoFisher). We found that the use of beads gave more consistent and

438 reproducible data than the use of water baths. After the temperature shift to inactivate GAL80ts, larvae
439 were returned to 18°C until dissection.
440
441 **Tissue preparation, staining and imaging**
442 For Acridine Orange staining, Larvae were dissected in PBS, and imaginal discs were incubated for 5 min
443 in PBS plus 0.5 mM AO (Sigma) at room temperature, washed twice with PBS, mounted in PBS, and
444 imaged immediately.
445 For γ-H2Av staining, larval wing discs were dissected in PBS, fixed in 2% paraformaldehyde (PFA)
446 in PBS for 45 min, and washed twice with PBS. Discs were permeabilized in PBS with 0.5% Triton X-100
447 for 12.5 min. For other antibodies, wing discs were dissected in PBS, fixed in 4% PFA in PBS for 30
448 minutes, and washed three times in PBS, permeabilized in PBS with 0.5% Triton X-100 for 10 min, and
449 rinsed in PBTx (0.1% Triton X-100). The discs blocked in 5% Normal Goal Serum in PBTx (0.1% Triton X-
450 100) for at least 1 h and incubated overnight at 4°C in primary antibody in block. Primary antibodies
451 used were to cleaved Dcp1 (1:100, rabbit polyclonal, Cell Signaling Cat# 9578), Phospho-Histone H3
452 (1:1000, rabbit monoclonal, Upstate Biotech), Wingless (1:100, mouse monoclonal, Developmental
453 Studies Hybridoma Bank Cat# 4D4) and γ-H2Av antibody (1:1000, mouse monoclonal, Developmental
454 Studies Hybridoma Bank Cat# UNC93-5.2.1, deposited to the DSHB by Hawley, R.S.). The discs were
455 rinsed thrice in PBTx (0.1% Triton X-100) and blocked for at least 30 min before incubation in secondary
456 antibody in block for 2 h at room temperature. Secondary antibodies were used at 1:400-500 (Jackson).
457 Stained discs were washed in PBTx and counter-stained with 10 ug/ml Hoechst33258 in PBTx for 2 min,
458 washed 3 times, and mounted on glass slides in Fluoromount G (SouthernBiotech).
459 For adult wings, newly eclosed adults that have yet to unfurl wings were collected and kept at
460 room temperature until the wings unfurl. The wings were collected within 30 min of unfurling,
461 submerged in PBTx, mounted in Fluoromount G (SouthernBiotech), and imaged immediately. Any delay,

462 we found, meant the loss of fluorescent signal as wing epithelial cells are eliminated in a
463 developmentally regulated wing maturation step [28, 29].
464 Wing discs and wings were imaged on a Leica DMR compound microscope using a Q-Imaging R6
465 CCD camera and Ocular or Micro-Manager software. Images were processed and analyzed using ImageJ
466 software.
467
468 **Statistical Analysis**
469 For sample size justifications, we used a simplified resource equation from [33]; E = Total number of
470 animals − Total number of groups, where E value of 10-20 is considered adequate. When we compare
471 two groups (-IR and +IR for example, where the former is the control group and the latter is the treated
472 group), n= 6 per group or E = 11 would be adequate. All samples subjected to statistical analysis exceed
473 this criterion. 2-tailed Student t-test with equal variance was used.
474
475 **Acknowledgements (include funding sources)**
476 *Drosophila* stocks from the Bloomington *Drosophila* Stock Center (NIH P40OD018537) were used in this
477 study. The authors thank Hardwick and Tang labs for Caspase Tracker stocks, Montell lab for CasExpress
478 stocks, and Kristin White for the critical reading of the manuscript. This work was funded by an NIH
479 grant and a diversity supplement to TTS (R35 GM130374) and a diversity supplement to support SCP
480 (R35 GM130374-S1). Monoclonal antibodies developed by Joshua Sanes, Stephen Cohen, and R. Scott
481 Hawley were obtained from the Developmental Studies Hybridoma Bank, created by the NICHD of the
482 NIH and maintained at The University of Iowa, Department of Biology, Iowa City, IA 52242.

483 **References**


484 1. Aram L, Yacobi-Sharon K, Arama E. CDPs: caspase-dependent non-lethal cellular processes. Cell
485 Death Differ. 2017;24(8):1307-10. Epub 2017/07/12. doi: 10.1038/cdd.2017.111. PubMed PMID:
486 28695898; PubMed Central PMCID: PMCPMC5520448.

487 2. Baena-Lopez LA. All about the caspase-dependent functions without cell death. Semin Cell Dev
488 Biol. 2018;82:77-8. Epub 2018/01/18. doi: 10.1016/j.semcdb.2018.01.005. PubMed PMID: 29339195.

489 3. Chakraborty S, Mir KB, Seligson ND, Nayak D, Kumar R, Goswami A. Integration of EMT and
490 cellular survival instincts in reprogramming of programmed cell death to anastasis. Cancer Metastasis
491 Rev. 2020;39(2):553-66. Epub 2020/02/06. doi: 10.1007/s10555-020-09866-x. PubMed PMID:
492 32020420.

493 4. Gudipaty SA, Conner CM, Rosenblatt J, Montell DJ. Unconventional Ways to Live and Die: Cell
494 Death and Survival in Development, Homeostasis, and Disease. Annu Rev Cell Dev Biol. 2018;34:311-32.
495 Epub 2018/08/09. doi: 10.1146/annurev-cellbio-100616-060748. PubMed PMID: 30089222; PubMed
496 Central PMCID: PMCPMC6791364.

497 5. Su TT. Non-apoptotic roles of apoptotic proteases: new tricks for an old dog. Open Biol.
498 2020;10(8):200130. Epub 2020/08/19. doi: 10.1098/rsob.200130. PubMed PMID: 32810419.

499 6. Tang HM, Tang HL. Anastasis: recovery from the brink of cell death. R Soc Open Sci.
500 2018;5(9):180442. Epub 2019/03/07. doi: 10.1098/rsos.180442. PubMed PMID: 30839720; PubMed
501 Central PMCID: PMCPMC6170572.

502 7. McArthur K, Kile BT. Apoptotic Caspases: Multiple or Mistaken Identities? Trends Cell Biol.
503 2018;28(6):475-93. Epub 2018/03/20. doi: 10.1016/j.tcb.2018.02.003. PubMed PMID: 29551258.

504 8. Nakajima YI, Kuranaga E. Caspase-dependent non-apoptotic processes in development. Cell
505 Death Differ. 2017;24(8):1422-30. Epub 2017/05/20. doi: 10.1038/cdd.2017.36. PubMed PMID:
506 28524858; PubMed Central PMCID: PMCPMC5520453.

507 9. Tang HL, Tang HM, Mak KH, Hu S, Wang SS, Wong KM, et al. Cell survival, DNA damage, and
508 oncogenic transformation after a transient and reversible apoptotic response. Mol Biol Cell.
509 2012;23(12):2240-52. Epub 2012/04/27. doi: 10.1091/mbc.E11-11-0926. PubMed PMID: 22535522;
510 PubMed Central PMCID: PMCPMC3374744.
511 10. Tang HM, Talbot CC, Jr., Fung MC, Tang HL. Molecular signature of anastasis for reversal of
512 apoptosis. F1000Res. 2017;6:43. Epub 2017/03/30. doi: 10.12688/f1000research.10568.2. PubMed
513 PMID: 28299189; PubMed Central PMCID: PMCPMC5310529.
514 11. Ichim G, Lopez J, Ahmed SU, Muthalagu N, Giampazolias E, Delgado ME, et al. Limited
515 mitochondrial permeabilization causes DNA damage and genomic instability in the absence of cell death.
516 Mol Cell. 2015;57(5):860-72. Epub 2015/02/24. doi: 10.1016/j.molcel.2015.01.018. PubMed PMID:
517 25702873; PubMed Central PMCID: PMCPMC4352766.
518 12. Liu X, He Y, Li F, Huang Q, Kato TA, Hall RP, et al. Caspase-3 promotes genetic instability and
519 carcinogenesis. Mol Cell. 2015;58(2):284-96. Epub 2015/04/14. doi: 10.1016/j.molcel.2015.03.003.
520 PubMed PMID: 25866249; PubMed Central PMCID: PMCPMC4408780.
521 13. Ding AX, Sun G, Argaw YG, Wong JO, Easwaran S, Montell DJ. CasExpress reveals widespread and
522 diverse patterns of cell survival of caspase-3 activation during development in vivo. Elife. 2016;5. Epub
523 2016/04/09. doi: 10.7554/eLife.10936. PubMed PMID: 27058168; PubMed Central PMCID:
524 PMCPMC4865370.
525 14. Tang HL, Tang HM, Fung MC, Hardwick JM. In vivo CaspaseTracker biosensor system for
526 detecting anastasis and non-apoptotic caspase activity. Sci Rep. 2015;5:9015. Epub 2015/03/12. doi:
527 10.1038/srep09015. PubMed PMID: 25757939; PubMed Central PMCID: PMCPMC4355673.
528 15. Evans CJ, Olson JM, Ngo KT, Kim E, Lee NE, Kuoy E, et al. G-TRACE: rapid Gal4-based cell lineage
529 analysis in Drosophila. Nat Methods. 2009;6(8):603-5. Epub 2009/07/28. doi: 10.1038/nmeth.1356.
530 PubMed PMID: 19633663; PubMed Central PMCID: PMC2754220.

531 16. Verghese S, Su TT. Ionizing radiation induces stem cell-like properties in a caspase-dependent
532 manner in Drosophila. PLoS Genet. 2018;14(11):e1007659. Epub 2018/11/22. doi:
533 10.1371/journal.pgen.1007659. PubMed PMID: 30462636; PubMed Central PMCID: PMCPMC6248896.
534 17. Wichmann A, Jaklevic B, Su TT. Ionizing radiation induces caspase-dependent but Chk2- and p53-
535 independent cell death in Drosophila melanogaster. Proc Natl Acad Sci U S A. 2006;103(26):9952-7. Epub
536 2006/06/21. doi: 10.1073/pnas.0510528103. PubMed PMID: 16785441; PubMed Central PMCID:
537 PMCPMC1502560.
538 18. Abrams JM, White K, Fessler LI, Steller H. Programmed cell death during Drosophila
539 embryogenesis. Development. 1993;117(1):29-43. Epub 1993/01/01. PubMed PMID: 8223253.
540 19. Wells BS, Johnston LA. Maintenance of imaginal disc plasticity and regenerative potential in
541 Drosophila by p53. Dev Biol. 2012;361(2):263-76. Epub 2011/11/01. doi: 10.1016/j.ydbio.2011.10.012.
542 PubMed PMID: 22036477; PubMed Central PMCID: PMCPMC3296280.
543 20. Neufeld TP, de la Cruz AF, Johnston LA, Edgar BA. Coordination of growth and cell division in the
544 Drosophila wing. Cell. 1998;93(7):1183-93. Epub 1998/07/10. doi: 10.1016/s0092-8674(00)81462-2.
545 PubMed PMID: 9657151.
546 21. Tozluoglu M, Duda M, Kirkland NJ, Barrientos R, Burden JJ, Munoz JJ, et al. Planar Differential
547 Growth Rates Initiate Precise Fold Positions in Complex Epithelia. Dev Cell. 2019;51(3):299-312 e4. Epub
548 2019/10/15. doi: 10.1016/j.devcel.2019.09.009. PubMed PMID: 31607650; PubMed Central PMCID:
549 PMCPMC6838681.
550 22. Florentin A, Arama E. Caspase levels and execution efficiencies determine the apoptotic
551 potential of the cell. J Cell Biol. 2012;196(4):513-27. Epub 2012/02/22. doi: 10.1083/jcb.201107133.
552 PubMed PMID: 22351928; PubMed Central PMCID: PMCPMC3283987.

553 23. Verghese S, Su TT. Drosophila Wnt and STAT Define Apoptosis-Resistant Epithelial Cells for
554 Tissue Regeneration after Irradiation. PLoS Biol. 2016;14(9):e1002536. doi:
555 10.1371/journal.pbio.1002536. PubMed PMID: 27584613; PubMed Central PMCID: PMCPMC5008734.
556 24. Moon NS, Frolov MV, Kwon EJ, Di Stefano L, Dimova DK, Morris EJ, et al. Drosophila E2F1 has
557 context-specific pro- and antiapoptotic properties during development. Dev Cell. 2005;9(4):463-75. Epub
558 2005/10/04. doi: 10.1016/j.devcel.2005.08.015. PubMed PMID: 16198289.
559 25. Bergmann A, Agapite J, McCall K, Steller H. The Drosophila gene hid is a direct molecular target
560 of Ras-dependent survival signaling. Cell. 1998;95(3):331-41. Epub 1998/11/14. doi: 10.1016/s0092-
561 8674(00)81765-1. PubMed PMID: 9814704.
562 26. Lu Q, Schafer DA, Adler PN. The Drosophila planar polarity gene multiple wing hairs directly
563 regulates the actin cytoskeleton. Development. 2015;142(14):2478-86. Epub 2015/07/15. doi:
564 10.1242/dev.122119. PubMed PMID: 26153232; PubMed Central PMCID: PMCPMC4510862.
565 27. Brown J, Bush I, Bozon J, Su TT. Cells with loss-of-heterozygosity after exposure to ionizing
566 radiation in Drosophila are culled by p53-dependent and p53-independent mechanisms. PLoS Genet.
567 2020;16(10):e1009056. Epub 2020/10/20. doi: 10.1371/journal.pgen.1009056. PubMed PMID:
568 33075096; PubMed Central PMCID: PMCPMC7595702.
569 28. Baker BS, Carpenter AT, Ripoll P. The Utilization during Mitotic Cell Division of Loci Controlling
570 Meiotic Recombination and Disjunction in DROSOPHILA MELANOGASTER. Genetics. 1978;90(3):531-78.
571 Epub 1978/11/01. doi: 10.1093/genetics/90.3.531. PubMed PMID: 17248870; PubMed Central PMCID:
572 PMCPMC1213905.
573 29. Sun G, Ding XA, Argaw Y, Guo X, Montell DJ. Akt1 and dCIZ1 promote cell survival from apoptotic
574 caspase activation during regeneration and oncogenic overgrowth. Nat Commun. 2020;11(1):5726. Epub
575 2020/11/14. doi: 10.1038/s41467-020-19068-2. PubMed PMID: 33184261; PubMed Central PMCID:
576 PMCPMC7664998.

577 30. Zhou L, Schnitzler A, Agapite J, Schwartz LM, Steller H, Nambu JR. Cooperative functions of the
578 reaper and head involution defective genes in the programmed cell death of Drosophila central nervous
579 system midline cells. Proc Natl Acad Sci U S A. 1997;94(10):5131-6. Epub 1997/05/13. doi:
580 10.1073/pnas.94.10.5131. PubMed PMID: 9144202; PubMed Central PMCID: PMCPMC24643.
581 31. Lawrence PA, Sanson B, Vincent JP. Compartments, wingless and engrailed: patterning the
582 ventral epidermis of Drosophila embryos. Development. 1996;122(12):4095-103. Epub 1996/12/01. doi:
583 10.1242/dev.122.12.4095. PubMed PMID: 9012529.
584 32. Verghese S, Bedi S, Kango-Singh M. Hippo signalling controls Dronc activity to regulate organ
585 size in Drosophila. Cell Death Differ. 2012;19(10):1664-76. Epub 2012/05/05. doi: 10.1038/cdd.2012.48.
586 PubMed PMID: 22555454; PubMed Central PMCID: PMCPMC3438497.
587 33. Charan J, Kantharia ND. How to calculate sample size in animal studies? J Pharmacol
588 Pharmacother. 2013;4(4):303-6. Epub 2013/11/20. doi: 10.4103/0976-500X.119726. PubMed PMID:
589 24250214; PubMed Central PMCID: PMCPMC3826013.
590
591

592 **Figure Legends**

593

594 **Figure 1. Optimizing temperature shift conditions to detect cells with X-ray-induced past caspase**

595 **activity**

596 Larvae were treated as in Fig. 1A where T= 29°, 26°, 22° or 18°C as indicated on the panels. Wing discs

597 were dissected at 72h after exposure to 0R (-IR) or 4000R (+IR), fixed, stained for DNA, and imaged for

598 DNA and GFP. CasTrk = Caspase Tracker. CasEx = CasExpress. The genotype of the wing discs shown was

599 CasExpress/G-trace; GAL80$^{ts}$/+ in all panels except (I) which shows a control CasExpress mutant with a

600 DQVD>DQVA mutation that renders the GAL4 membrane tether caspase-resistant. Scale bar = 120

601 microns.

602 (A) The experimental protocol

603 (B) Fractional area of each disc that is GFP+ was quantified in Image J. p-values were calculated

604 using a 2-tailed t-test. The numbers in the brackets are the number of discs analyzed in two to four

605 biological replicate experiments per sample.

606 (C-C') An unirradiated disc shows GFP+ cells even after a short (6h) pulse of heat inactivation of

607 GAL80$^{ts}$ at 29°C.

608 (D-D') An irradiated disc shows more GFP+ cells with the same temperature shift as in C.

609 (E-G') Unirradiated discs show few GFP+ cells when the temperature shift for 6h is to 18°C (E),

610 22°C (F) or 26°C (G-G').

611 (H-H') A irradiated discs from larvae shifted to 26°C shows robust GFP signal.

612 (I) Discs from caspase-resistant CasExpress mutant larvae treated exactly as in H.

613 (J) Discs from larvae treated exactly as in (H) but with no temperature shift

614

615

616 **Figure 2. XPAC cells are capable of proliferating**

617 Larvae of the genotype CasExpress/G-trace; GAL80$^{ts}$/+ were treated as in Fig. 1A where T=26°C. Wing
618 discs were dissected at 24, 48 and 72h after exposure to 4000R, fixed, and stained for DNA. The discs
619 were imaged for GFP (A-C), DNA (A'-C') and RFP (A''-C''). N= number of discs examined in three
620 biological replicates for 24h and 2 biological replicates each for 48 and 72h. The arrow points to a singlet
621 GFP+ cell and the arrowhead points to a doublet of GFP+ cells in panel A. Scale bar = 120 microns.

622

623 **Figure 3. XPAC prevalence in development and the effect of apoptotic signaling**

624 Larvae of the genotype CasExpress/G-trace; GAL80$^{ts}$/+ were treated as in Fig. 1A where T=26°C. Wing
625 discs were dissected at 24h after exposure to 4000R, fixed, and stained for DNA. Scale bar = 120
626 microns. p-values were calculated using a 2-tailed t-test.

627 (A-D') The discs were imaged for DNA (A-D) or GFP (A'-D'). Hinge folds are visible in DNA images
628 of more developed discs and are indicated with arrowheads in (C-D). n = notum and w = future wing that
629 includes the hinge and the pouch. The most distal region of the future wing is indicated with * in (A'-C');
630 GFP+ cells clear from this region before the rest of the future wing. A ring of GFP+ cells is indicated with
631 arrows (C').

632 (E-E') CasExpress/G-trace; GAL80$^{ts}$/+ larvae that also carried one copy of UAS-hid, rpr on the X
633 chromosome were treated as in (A-D).

634 (F) The % of disc area that is GFP+ was quantified from discs such as those shown in A'-D' and
635 plotted against the total disc area. The numbers of discs analyzed are in parentheses. The data are from
636 3 (6-7d) and 2 (7-8d) biological replicates each.

637 (G) The % of disc area that is GFP+ was quantified for discs with no epithelial folds (less
638 developed discs such as those in A and B) and discs with epithelial folds (more developed discs such as
639 those in C and D). The data are from 6 biological replicate samples of larvae 7-8d old at irradiation.

640 (H-I) The % of disc area that is GFP+ was quantified from discs such as those shown in E' and

641 plotted against the total disc area. The number of discs analyzed are in parentheses.

642 The genotypes were:

643 Control = CasExpress/G-trace; GAL80$^{ts}$/+

644 hid, rpr = UAS-hid, UAS-rpr/+ or Y; CasExpress/G-trace; GAL80$^{ts}$/+

645 rpr = UAS-rpr/+ or Y; CasExpress/G-trace; GAL80$^{ts}$/+

646 DroncDN = CasExpress/G-trace; GAL80$^{ts}$/UAS-Dronc$^{DN}$

647 H99 = CasExpress/G-trace; GAL80$^{ts}$/H99

648 p35 = CasExpress/G-trace; GAL80$^{ts}$/UAS-p35

649

650 **Figure 4. Apoptosis and mitosis are widespread throughout the wing disc**

651 The larvae of the genotype CasExpress/G-trace; GAL80$^{ts}$/+ were treated as in Fig. 1A where T=26°C.

652 Scale bar = 120 microns.

653 (A-C'') Wing discs were fixed and stained with an antibody to phospho-S10 on Histone H3, a

654 mitotic marker. The dashed line marks the pouch. The discs were also stained for DNA and visualized for

655 CasExpress>GFP. The arrows point to the notum and the dashed lines mark the pouch.

656 (D-F''') Wing discs were fixed and stained with an anti-cleaved-Dcp1 antibody to detect cells that

657 activated apoptotic caspases. The discs were also stained for DNA and visualized for CasExpress>GFP.

658 The arrows point to the notum and the * marks the distal pouch.

659 (G-J) Wing discs were stained live with the vital dye Acridine Orange which reports on apoptotic

660 cells. The brackets mark the hinge region that is resistant to IR-induced apoptosis. The arrows point to

661 the notum and the * marks the distal pouch.

662

663 **Figure 5. Developmental signaling pathways regulate XPAC cell prevalence**

664 (A-E') Larvae of the genotypes indicated below were treated as in Fig. 1A where T=26°C. The
665 discs were dissected 24h after exposure to 4000R, fixed and stained with an antibody against Wg (A-
666 D'''). The discs were also stained for DNA and visualized for CasExpress>GFP. Arrows indicate the notum
667 and * indicate the distal pouch. Arrowheads indicate the Wg Inner Ring (white) or the D/V boundary
668 (yellow).
669 (F-G) The GFP+ areas were quantified and expressed as % of the total disc area. p-values were
670 calculated using a 2-tailed t-test. Scale bar = 120 microns. The genotypes were:
671 Control = CasExpress/G-trace; GAL80$^{ts}$/+
672 wg = CasExpress/G-trace; GAL80$^{ts}$/UAS-wg
673 Axin = CasExpress/G-trace; GAL80$^{ts}$/UAS-Axin
674 NotchICD = CasExpress/G-trace; GAL80$^{ts}$/UAS-N$^{ICD}$
675 mam-delta = CasExpress/G-trace; GAL80$^{ts}$/UAS-mam$^{\Delta}$
676 RasV12 = CasExpress/G-trace; GAL80$^{ts}$/UAS-Ras$^{V12}$
677
678 **Figure 6. Cells with past caspase activity show reduced IR-induced LOH**
679 (A-F) Adult wings from larvae of the genotype CasExpress/G-trace; GAL80$^{ts}$/mwh$^{1}$. The
680 experimental protocol shown in Fig. 1A was followed but larvae were aged for 6d at 18°C after egg
681 collection to get 6-7d old larvae (A-C) or aged for 7d at 18°C after egg collection to get 7-8d old larvae at
682 the time of irradiation. Larvae were irradiated with 0 or 4000R of X-rays. After incubation at 26°C, larvae
683 were returned to 18°C for the remainder of the experiment. The two +IR wings shown for each group
684 represent the range of clone size and number observed in two biological replicate experiments. The
685 number of wings examined was 12 (6-7d -IR) , 9 (6-7d +IR). 6 (7-8d -IR) and 11 (7-8d +IR), in two
686 biological replicate experiments each.

687 (G) A region of the wing was imaged at 4X magnification relative to A-F. It is possible to discern
688 the top (in focus, arrow) and the bottom (out-of-focus, arrowhead) surfaces of the wing in such images.
689 (H) A region of the wing is shown magnified 16X relative to A-F. It is possible to assign mwh state
690 to individual GFP+ cells, for example, 3 cells within dashed lines. In a patch of mwh cells (white line),
691 none are GFP+.
692 (I) Percent of image area that is mwh was quantified from images such as G, for the GFP+ and
693 GFP- portion of the surface in focus. The data include wings from animals irradiated as 6-7d (gray) or 7-
694 8d (black) old larvae. Each dataset also shows a significant difference in mwh between GFP- and GFP+
695 areas: p= 0.04 for 6-7d and 0.03 for 7-8d. p-values were computed using a 2-tailed t-test.
696 (J-K'''') Larvae of the genotype CasExpress/G-trace; GAL80$^{ts}$/+ were treated as in Fig. 1A. Wing
697 discs were dissected at 20-22h after irradiation with 4000R, fixed and stained with an antibody against γ-
698 H2Av. The discs were also stained for DNA and imaged for GFP. Arrowheads in J'''' indicate rare cells in
699 which GFP and γ-H2Av signals overlap to appear white. The boxed area in J''' is magnified in K-K''''. L-L'''
700 show a magnified area of another disc, to demonstrate reproducibility. A total of 52 discs were
701 examined in 3 biological replicate experiments.
702 Scale bar = 960 microns in A-F, 120 microns in J and 48 microns in K-L.
703
704 **S1 Figure. Caspase cleavage without IR and DNA double strand breaks with and without IR.**
705 Larvae of the genotype CasExpress/G-trace; GAL80ts/+ were treated as in Fig. 1A where T=26°C. Wing
706 discs were dissected at 4h after exposure to 0 or 4000R of X-rays, fixed, and stained for DNA and with
707 antibodies to cleaved Dcp1 (A-A') or γ-H2Av (B-C'). The scale bar = 120 microns in A and 24 microns in B-
708 C.
709
710 **S1 Table. Fly stocks used.**

# FIGURE 1

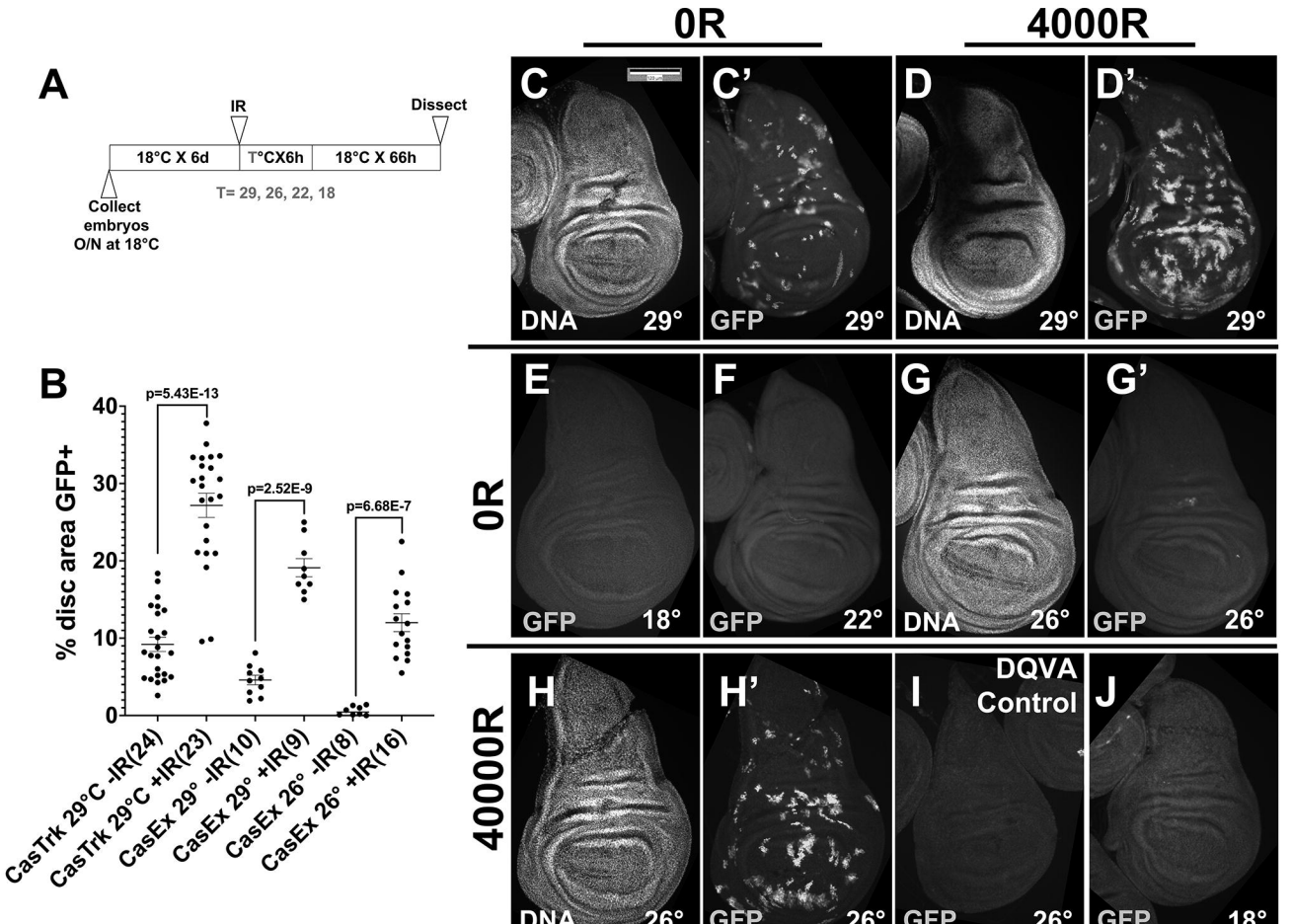
A
IR
Dissect
18°C X 6d
T°CX6h
18°C X 66h
T= 29, 26, 22, 18
Collect embryos O/N at 18°C
B
% disc area GFP+
p=5.43E-13
p=2.52E-9
p=6.68E-7
CasTrk 29°C -IR(24)
CasTrk 29°C +IR(23)
CasEx 29° -IR(10)
CasEx 29° +IR(9)
CasEx 26° -IR(8)
CasEx 26° +IR(16)
0R
4000R
C
C'
D
D'
DNA 29°
GFP 29°
DNA 29°
GFP 29°
0R
E
F
G
G'
GFP 18°
GFP 22°
DNA 26°
GFP 26°
40000R
H
H'
I
J
DQVA Control
DNA 26°
GFP 26°
GFP 26°
GFP 18°

# FIGURE 2

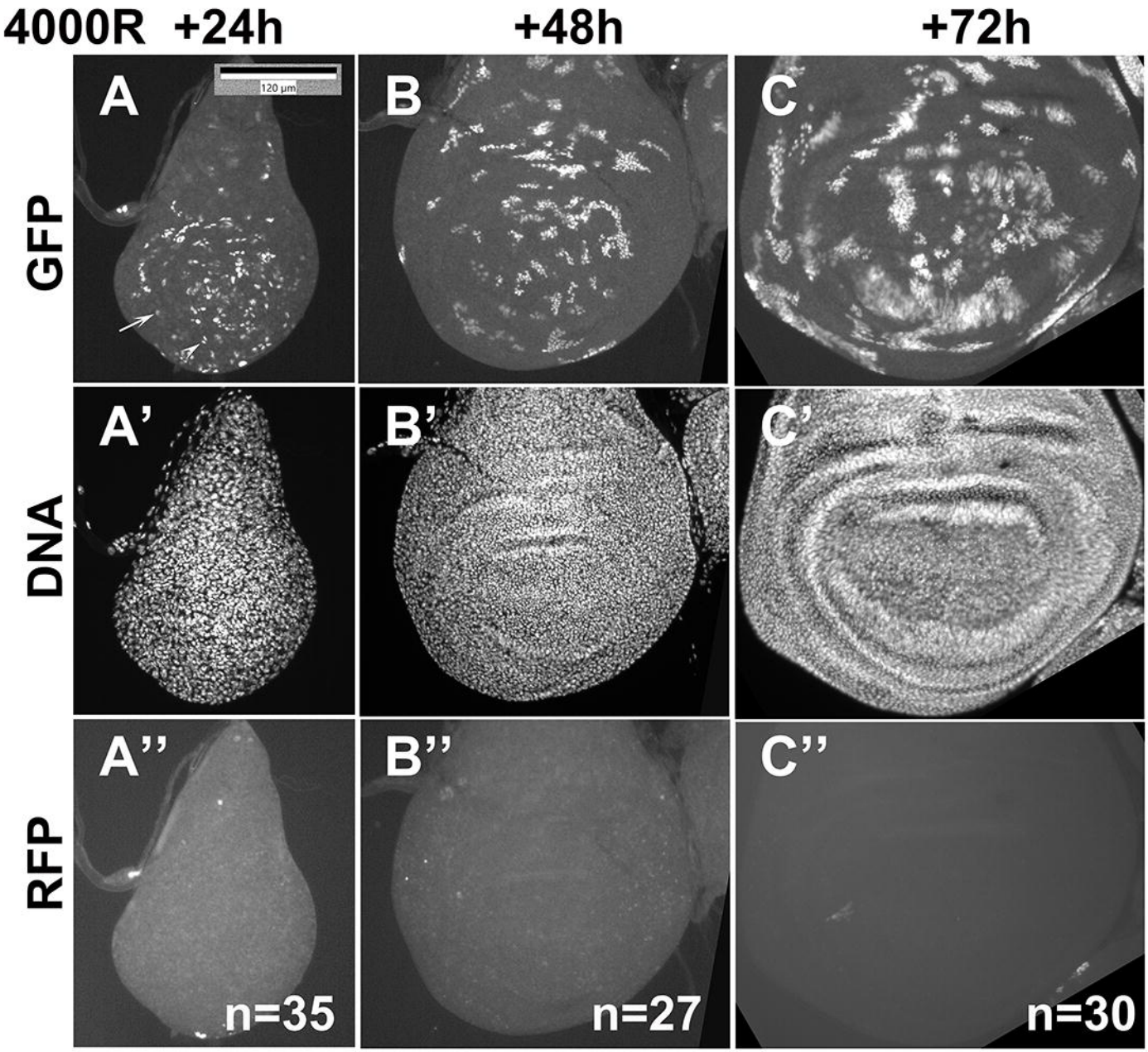

# FIGURE 3

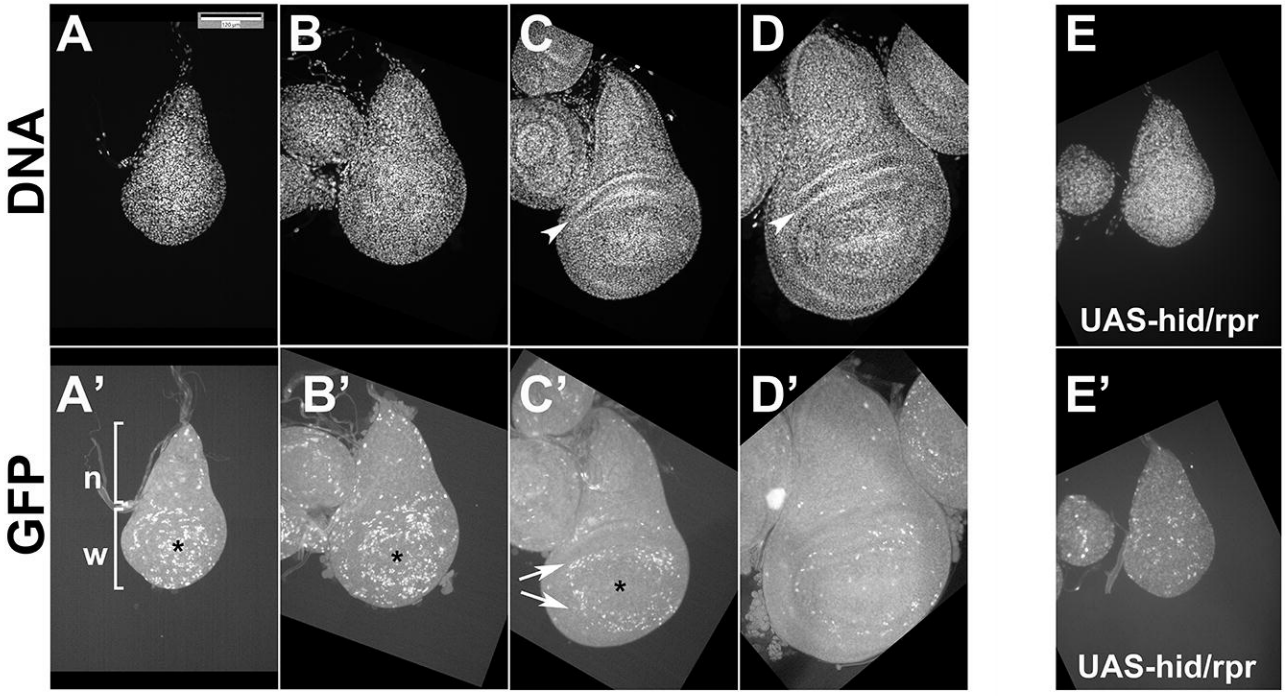
DNA
GFP
A
B
C
D
E
UAS-hid/rpr
A'
B'
C'
D'
E'
n
w
*
UAS-hid/rpr

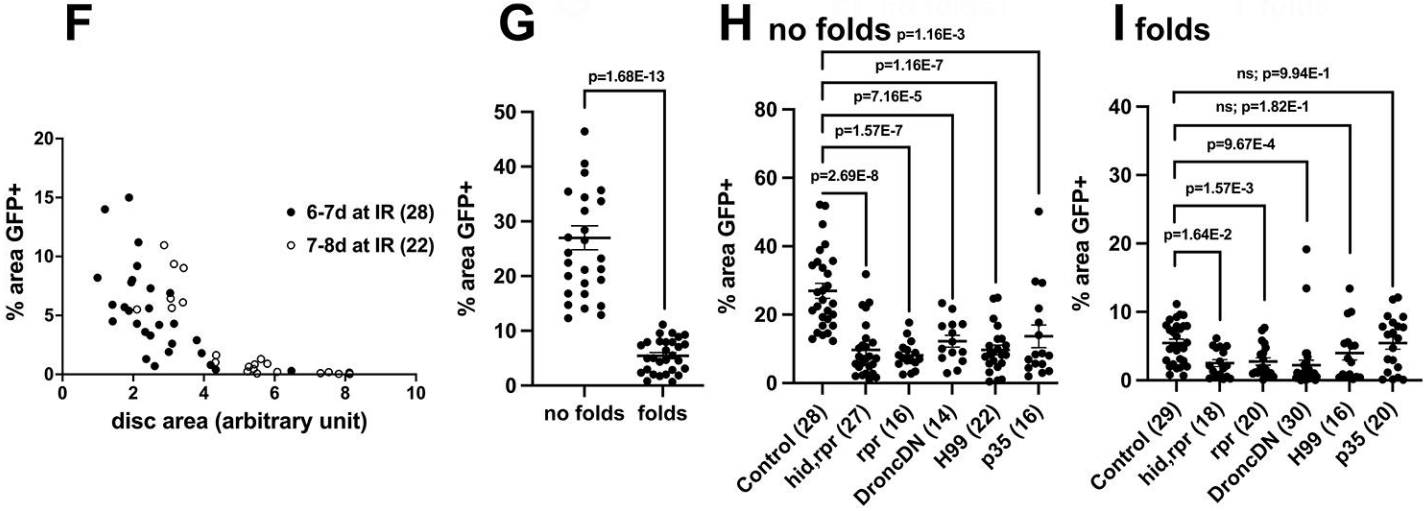
F
% area GFP+
disc area (arbitrary unit)
6-7d at IR (28)
7-8d at IR (22)
G
p=1.68E-13
% area GFP+
no folds
folds
H no folds
p=1.16E-3
p=1.16E-7
p=7.16E-5
p=1.57E-7
p=2.69E-8
% area GFP+
Control (28)
hid,rpr (27)
rpr (16)
DroncDN (14)
H99 (22)
p35 (16)
I folds
ns; p=9.94E-1
ns; p=1.82E-1
p=9.67E-4
p=1.57E-3
p=1.64E-2
% area GFP+
Control (29)
hid,rpr (18)
rpr (20)
DroncDN (30)
H99 (16)
p35 (20)

# FIGURE 4

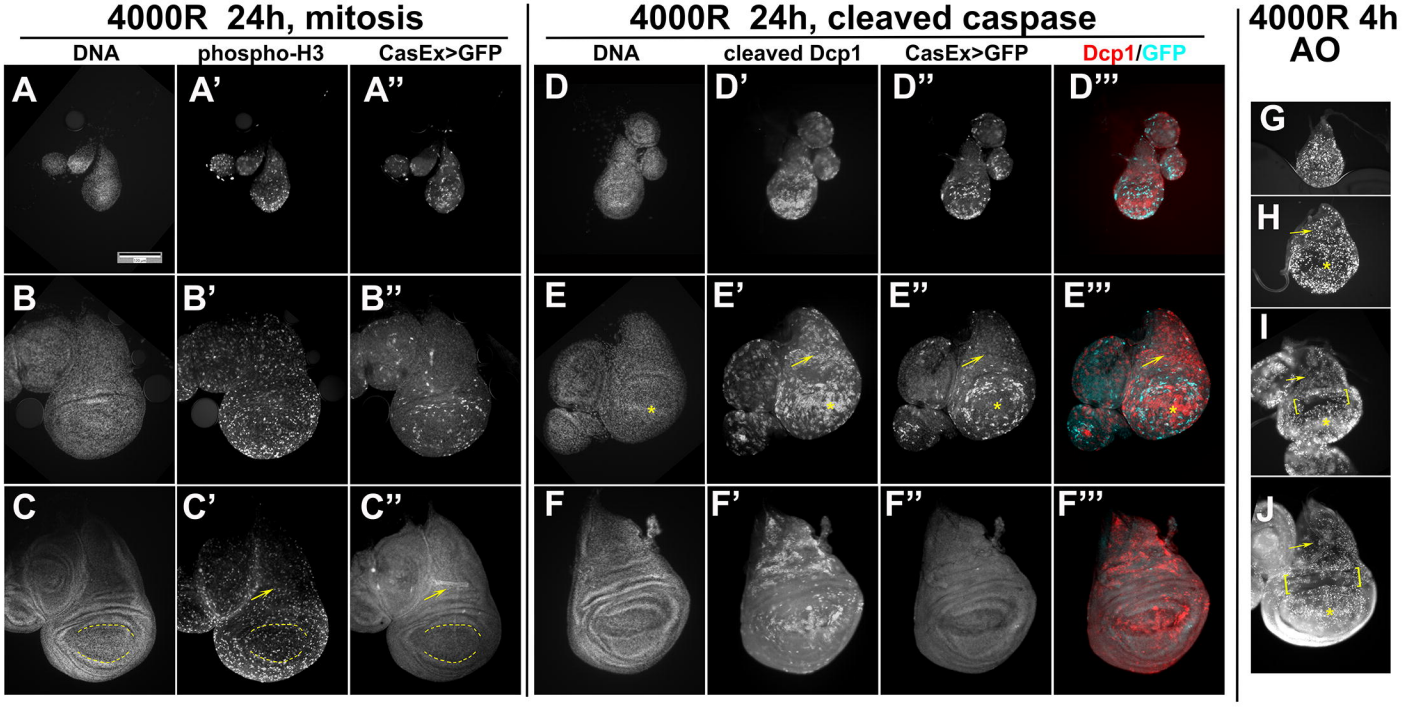
4000R 24h, mitosis
DNA
phospho-H3
CasEx>GFP
A
A'
A''
B
B'
B''
C
C'
C''
4000R 24h, cleaved caspase
DNA
cleaved Dcp1
CasEx>GFP
Dcp1/GFP
D
D'
D''
D'''
E
E'
E''
E'''
F
F'
F''
F'''
4000R 4h AO
G
H
I
J

# FIGURE 5

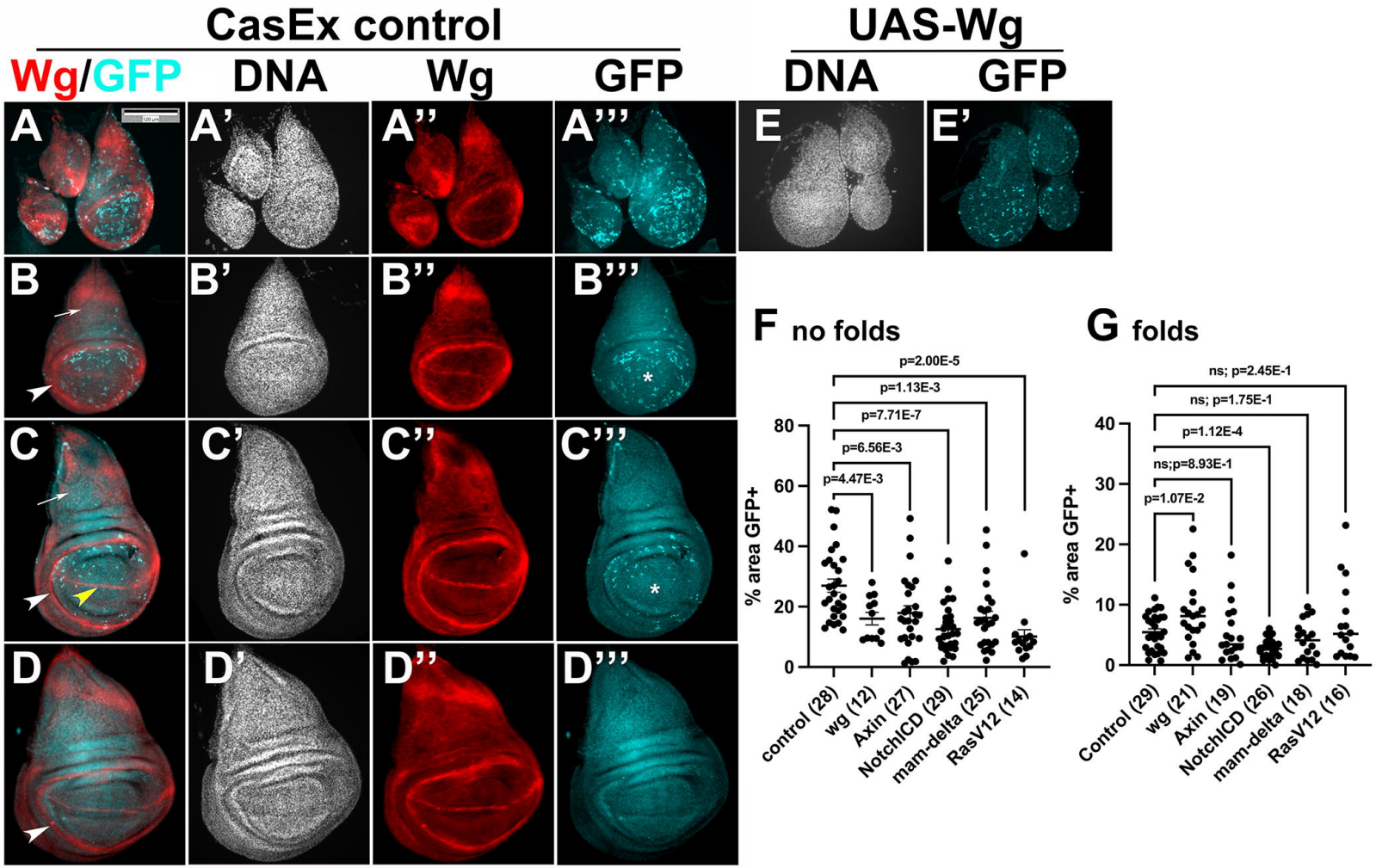
CasEx control
UAS-Wg
Wg/GFP
DNA
Wg
GFP
DNA
GFP
A
A'
A''
A'''
E
E'
B
B'
B''
B'''
C
C'
C''
C'''
D
D'
D''
D'''
F no folds
% area GFP+
p=2.00E-5
p=1.13E-3
p=7.71E-7
p=6.56E-3
p=4.47E-3
control (28)
wg (12)
Axin (27)
NotchICD (29)
mam-delta (25)
RasV12 (14)
G folds
% area GFP+
ns; p=2.45E-1
ns; p=1.75E-1
p=1.12E-4
ns;p=8.93E-1
p=1.07E-2
Control (29)
wg (21)
Axin (19)
NotchICD (26)
mam-delta (18)
RasV12 (16)

# FIGURE 6

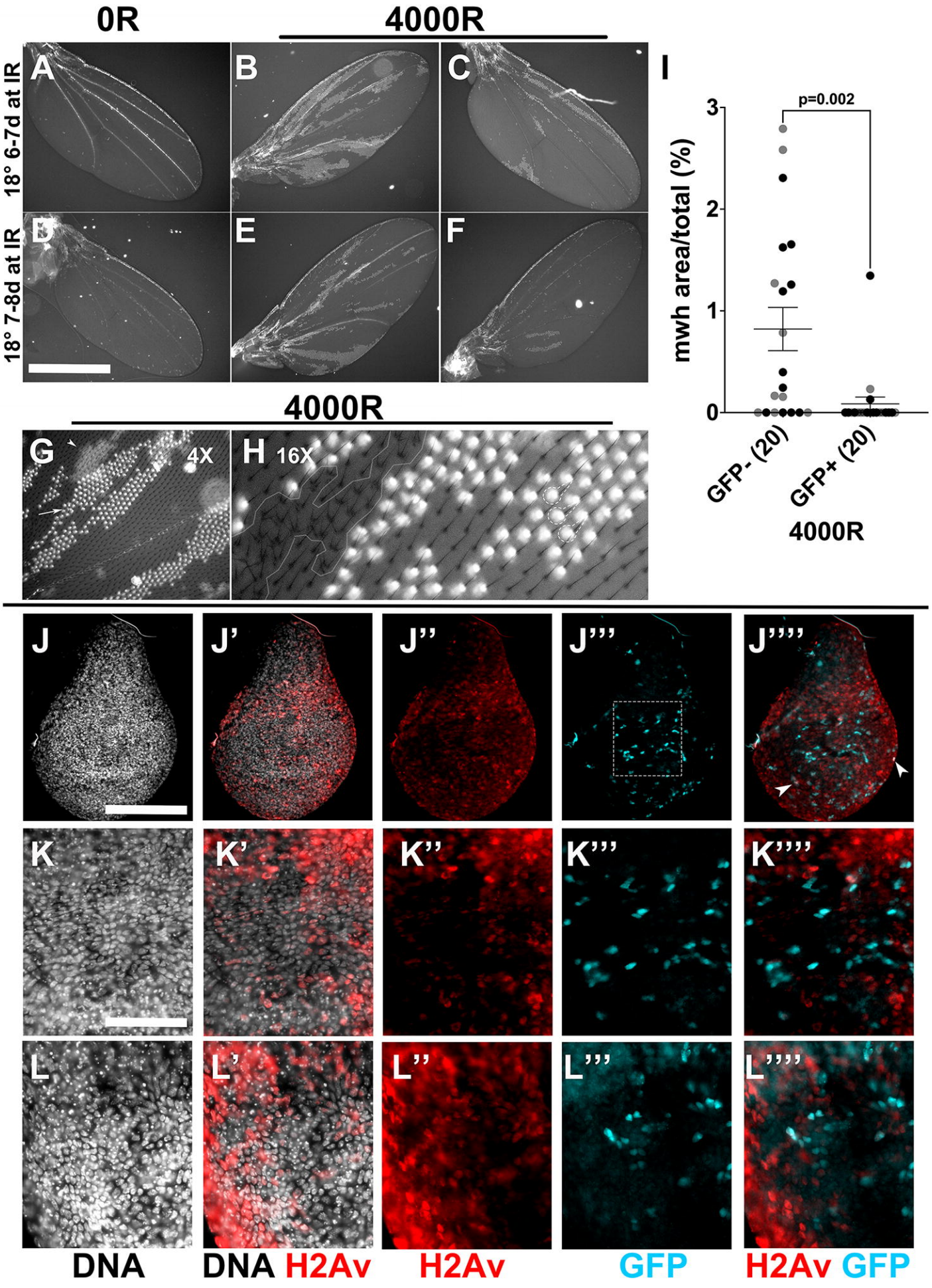
0R
4000R
18° 6-7d at IR
18° 7-8d at IR
A
B
C
D
E
F
I
p=0.002
mwh area/total (%)
3
2
1
0
GFP- (20)
GFP+ (20)
4000R
4000R
G
4X
H
16X
J
J'
J''
J'''
J''''
K
K'
K''
K'''
K''''
L
L'
L''
L'''
L''''
DNA
DNA H2Av
H2Av
GFP
H2Av GFP